Carbohydrate Polymers 114 (2014) 484–492

Contents lists available at ScienceDirect

Carbohydrate Polymers

journal homepage: www.elsevier.com/locate/carbpol

Properties and characterization of agar/CuNP bionanocomposite films prepared with different copper salts and reducing agents

Shiv Shankar, Xinnan Teng, Jong-Whan Rhim *

Department of Food Engineering and Bionanocomposite Research Institute, Mokpo National University, 61 Dorimri, Chungkyemyon, Muangun, 534-729 Jeonnam, Republic of Korea

ARTICLE INFO

Article history:
Received 8 July 2014
Received in revised form 8 August 2014
Accepted 19 August 2014
Available online 27 August 2014

Keywords:
Different copper salts
Reducing agents
Copper nanoparticle
Agar
Bio-nanocomposite film
Antimicrobial activity

ABSTRACT

Various types of agar-based bio-nanocomposite (BNC) films were prepared by blending agar and six different copper nanoparticles (CuNPs) with different shapes and sizes obtained from three different sources of copper salts and two different reducing agents. The BNC films were characterized by UV–visible, FE-SEM, FT-IR, and XRD. The thermogravimetric study showed that the melting point of BNC films was increased when ascorbic acid was used as a reducing agent for CuNPs synthesis. Apparent surface color and transmittance of agar film was greatly influenced by the reinforcement of CuNPs. However, mechanical and water vapor barrier properties did not change significantly ($p > 0.05$) by blending with CuNPs. Tensile modulus and tensile strength decreased slightly for all types of CuNPs reinforced while elongation at break slightly increased when CuNPs produced by ascorbic acid were blended. The agar bio-nanocomposite films showed profound antibacterial activity against both Gram-positive and Gram-negative food-borne pathogenic bacteria.

1. Introduction

Nanotechnology is a rapid growing field with multifaceted applications of new materials at the nanoscale level. Materials blended with various types of nanomaterials create enhanced material properties due to interfacial interactions between nanoscaled architectures which have a great potential in optical, electrical, medical, antibacterial applications (Drelich, Bowen, Hwang, Mills, & Hoffman, 2011; Huang et al., 1997; Liu & Bando, 2003; Magdassi, Grouchko, & Kamyshny, 2010). Research on biopolymer-based nanocomposite food packaging materials have been increased drastically owing to the biocompatibility, biodegradability, and environmentally friendliness (Duncan, 2011; Kanmani & Rhim, 2014a). However, biopolymer-based packaging materials have not been widely used in the packaging industry, because of their poor mechanical and processing properties as well as higher production cost (Tunc & Duman, 2011). As one of the ways to overcome such limitations, research works have been focused on developing bio-nanocomposite (BNC) materials by homogeneous blending of various types of nano-sized filler materials with biopolymers to improve the physical, mechanical, ultra violet light absorbing, gas barrier, and antimicrobial properties of the films. Antimicrobial packaging systems have been emerged as one of the most promising smart packaging systems which help to extend the shelf life of food by destroying or inhibiting spoilage and pathogenic micro-organisms that contaminate foods (Rhim, Wang, & Hong, 2013). BNC food packaging material with antimicrobial properties are particularly effective because of high surface to volume ratio of nanoparticles and enhances surface reactivity compared to bulk counterpart (Rhim, Wang, & Hong, 2013).

Metallic nanoparticles are one of the most promising type of nanomaterials for antimicrobial food packaging applications as they show strong antimicrobial activity due to their large surface area and high specificity (Gong et al., 2007). The antibacterial properties of metallic nanoparticles, such as copper and silver nanoparticles have attracted considerable attention in not only food packaging field, but also biomedical and biotechnological applications (Kyriacou, Brownlow, & Xu, 2004). Copper-based nanomaterials have advantageous over silver nanoparticles because of the low cost of source materials, insignificant sensitivity to human tissues, and highly sensitive to micro-organisms (Hostynek & Maibach, 2004). Copper ions and copper complexes have been used as effective materials for sterilizing liquids, and as antibacterial, antifungal and antiviral since ancient times (Borkow & Gabbay, 2009).

* Corresponding author. Tel.: +82 61 450 2423; fax: +82 61 454 1521.
E-mail addresses: jwrhim@mokpo.ac.kr, jwrhim@hanmail.net (J.-W. Rhim).

http://dx.doi.org/10.1016/j.carbpol.2014.08.036
0144-8617/

Various chemical, physical, and biological synthesis of copper nanoparticles have been reported in the literature (Dang, Le, Fribourg-Blanc, & Dang, 2011; Tilaki, Iraji zad, & Mahdavi, 2007; Vellora, Padil, & Černík, 2013). However, few reports are available on the green synthesis of copper nanoparticles (CuNPs) and on the preparation of CuNPs-based BNC films (Cardenas, Díaz, Meléndrez, Cruzat, & García, 2009; Mary, Bajpai, & Chand, 2009). In the present study, the CuNPs were synthesized using three different copper salts (copper acetate, copper chloride, and copper sulfate) and two different types of reducing agents (sodium hydroxide and ascorbic acid) to obtain various types of CuNPs with different shape and size. These CuNPs were used as reinforcing materials in agar to obtain agar/CuNPs BNC film. The CuNPs and agar/CuNPs composite films were characterized and the film properties were evaluated based on the type of CuNPs.

2. Material and methods

2.1. Chemicals

All chemicals were procured from Sigma-Aldrich (St. Louis, MO, USA) unless otherwise stated. Food-borne pathogenic bacteria, *Escherichia coli* O157:H7 ATCC 43895 and *Listeria monocytogenes* ATCC 15313, were obtained from Korean Collection for Type Cultures (KCTC, Seoul, Korea). The bacterial strains were cultured in tryptic soy broth (TSA) and brain heart infusion broth (BHI) agar media and subsequently stored at 4 °C for further analysis.

2.2. Synthesis of CuNPs

CuNPs were synthesized using copper acetate, copper chloride, and copper sulfate as precursors and sodium hydroxide (NaOH) and ascorbic acid (AA) as reducing agents (Shankar & Rhim, 2014). Fifty milliliters of 0.2 M copper acetate, copper chloride, or copper sulfate solutions were heated to 80 °C and added 50 mL of 0.6 M NaOH or 1 M AA solution dropwise while mixing with magnetic stirrer. The reaction mixtures were continued heating at 80 °C until dark solution was obtained.

The reaction products of copper precursors and NaOH were centrifuged at 8,000 rpm for 20 min. The precipitates were washed with distilled water and absolute ethanol for several times and dried at 60 °C for 6 h to obtain the dry powder of CuNPs. The CuNPs formed using copper acetate, copper chloride and copper sulfate as precursor and NaOH as reducing agents were designated as CuA^{NaOH}, CuC^{NaOH}, and CuS^{NaOH}, respectively.

The reaction products of copper precursors and AA were in dark solutions form, which were dialyzed overnight. The CuNPs synthesized by copper acetate, copper chloride, and copper sulfate were designated as CuA^{AA}, CuC^{AA}, and CuS^{AA}, respectively.

2.3. Synthesis of agar/CuNPs composite films

Agar/CuNPs BNC films were prepared by solution casting method following the method of Rhim et al. (2013). Briefly, 60 mg (2 wt% of agar) of CuNPs were mixed in 150 mL distilled water by constant stirring for 30 min. Then, glycerol (0.9 g) as plasticizer was added into the nanoparticles solutions with stirring for 20 min. Thereafter, 3 g of agar was added slowly into the nanoparticles solution with stirring and boiling until they dissolved completely. The film forming solutions were cast evenly onto a leveled Teflon film (Cole-Parmer Instrument Co., Chicago, IL, USA) coated glass plate (24 × 30 cm), and allowed to dry at room temperature (23 ± 2 °C) for 2 days. The dried films were peeled off from the plates and preconditioned at 25 °C and relative humidity (RH) of 50% for 48 h in the constant temperature humidity chamber to normalize the moisture content of the films prior to further characterization. The control agar film was prepared by the same method without addition of CuNPs. The films were designated as agar/CuA^{NaOH}, agar/CuC^{NaOH}, agar/CuS^{NaOH}, agar/CuA^{AA}, agar/CuC^{AA}, and agar/CuS^{AA} BNC films for respective CuNPs used.

2.4. Characterization of agar/CuNPs BNC films

2.4.1. Morphological observation

Field emission scanning electron microscopy (FE-SEM) analysis was performed to observe the microstructure of the film samples. Small piece of film samples was mounted on an SEM specimen holder and analyzed using a field emission scanning electron microscopy (FE-SEM, S-4800, Hitachi Co., Ltd., Matsuda, Japan) with an accelerating voltage of 5.0 kV.

2.4.2. FT-IR and XRD analysis

Fourier transform infrared (FT-IR) spectra of the films were obtained using an attenuated total reflectance-Fourier transform infrared (AT-FTIR) spectrophotometer (TENSOR 37 spectrophotometer with OPUS 6.0 software, Billerica, MA, USA) operated at a resolution of 4 cm^{-1}. Film samples were cut into rectangular shapes (5 cm × 5 cm) and directly placed on the ray exposing stage. The spectrum was recorded at wave number of 500–4000 cm^{-1}.

X-ray diffraction (XRD) pattern of the films was analyzed by X-ray diffractometer (PANalytical X'pert pro MRD diffractometer, Amsterdam, Netherlands). Samples were prepared by placing rectangular shapes of each film (2.5 × 2.5 cm) on a glass slide and the spectra were recorded using Cu Kα radiation (wavelength of 0.1541 nm) and a nickel monochromator filtering wave at 40 kV and 30 mA. The diffraction pattern was obtained at diffraction angles between 2θ = 30–80° with scanning speed of 0.4° min^{-1} at room temperature.

2.4.3. Measurement of surface color

The surface color of the films was measured using a Chroma meter (Konica Minolta, CR-400, Tokyo, Japan) with a white color plate (L = 97.75, a = −0.49, and b = 1.96) as a standard background for color measurement. Hunter color values (L, a, and b) were determined by taking an average of five readings from each film sample. Total color difference (ΔE) was calculated as follows: $\Delta E = [(\Delta L)^2 + (\Delta a)^2 + (\Delta b)^2]^{0.5}$ where ΔL, Δa, and Δb are the difference between each color value of standard color plate and film samples, respectively.

2.4.4. Optical properties

Optical properties of the films were determined by measuring light absorption spectra and the transparency of the films. Each film was cut into a rectangular piece and directly mounted between two spectrophotometer magnetic cells. Both the absorbance and percent transmittance spectra were measured using a UV–vis spectrophotometer (Mecasys Optizen POP Series UV/Vis, Korea). Absorbance was taken in the wavelength of 200–700 nm. Transparency of the films was tested by measuring percent transmittance at 280 nm (T_{280} nm) and 660 nm (T_{660} nm).

2.4.5. Water vapor permeability

The water vapor permeability (WVP) of the films was determined gravimetrically according to the standard method of ASTM E96-95 with slight modification (Gennadios, Weller, & Gooding, 1994). The WVP measuring cups were made of polymethylmethacrylate with inside depth and diameter of 2.5 and 6.8 cm, respectively. The films were cut into square pieces (7.5 cm × 7.5 cm) and directly mounted horizontally on the top of WVP measuring cups containing 18 mL of water. The level of water should be up to 1 cm underneath the film and each cup with the film

was tightened with screw to prevent leakage of water vapor. The cups were weighted and subsequently placed in an environmental chamber controlled at 25 °C and 50% RH with air current movement at 198 m min^{-1}. The cup was weighed every hour for a period of 8 h and weight loss from each cup was measured. Water vapor transmission rate (WVTR) was calculated from the slopes (linear) of the steady state portion of weight loss of the cup versus time curve. Then, the WVP of the films in g m m^{-2} s^{-1} Pa^{-1} was calculated as follows:

$$\mathrm{WVP} = \frac{\mathrm{WVTR} \times L}{\Delta p}$$

where WVTR was the measured water vapor transmission rate (g m^{-2} s^{-1}) through a film, L was the mean thickness of the film (m), and Δp was the partial water vapor pressure difference (Pa) across the film.

2.4.6. Water contact angle and moisture content

The surface hydrophobicity of the films was determined by measuring the water contact angle (WCA) of the film surface using a WCA analyzer (model Phoenix 150, Surface Electro Optics Co., Ltd., Kunpo, Korea). Briefly, each film was cut into rectangular pieces (3 cm × 10 cm) and directly placed on the horizontal movable stage (Black Teflon coated steel, 7 cm × 11 cm) fixed with the contact angle analyzer. The drop of water (~10 μL) was placed on the surface of the film using a micro syringe and contact angle was measured on both sides of the water drop to assume symmetry and horizontal level (Rhim, Hong, Park, & Ng, 2006). Three measurements were taken for each sample and the average values were presented as the degree of WCA.

The moisture content (MC) of the films was determined according to the method described (Rhim & Wang, 2013). For analysis, each film was cut into 3 cm × 3 cm and dried at 100 °C for 24 h using a hot air oven. The weight loss of each film was measured as MC and expressed as percent MC based on the initial weight of the film.

2.4.7. Thickness and tensile properties of the films

Thickness of the film samples was measured using a handheld micrometer (Dial Thickness Gauge 7301, Mitutoyo Corporation, Kanagawa, Japan) with an accuracy of 0.01 mm. Five random measurements were taken for each film and the average values were used as the film thickness. Tensile properties such as tensile strength (TS), elongation at break (E), and elastic modulus (EM) of each film were measured according to the standard test method of ASTM D 882-88 using Instron Universal Testing Machine (Model 5565, Instron Engineering Corporation, Canton, MA, USA). For this, each film was cut into rectangular strips (2.54 cm × 15 cm) using a precision double blade cutter (Model LB.02/A, Metrotech, SA, San Sebastain, Spain). The machine was operated in tensile mode with an initial grip separation of 50 mm and crosshead speed of 50 mm min^{-1}. The TS was expressed as Pa, and it was determined by dividing the maximum load (N) by the initial cross-sectional area (m^2) of the films. The E was expressed as percent, and it was determined by dividing the extension at the rupture of the film by the initial length of the film (50 mm) multiplied by 100, and the EM (GPa) was determined from the slope of the linear portion of the stress–strain curve, which corresponds to the stress divided by the strain of the film sample. Ten measurements were carried out for each film and the average values were presented.

2.4.8. Thermal stability

Thermal stability of the films was determined using a thermogravimetric analyzer (TGA; Hi-Res TGA 2950, TA Instrument, New Castle, DE, USA). Each film sample (about 5 mg) was taken in a standard aluminum cup and scanned at a heating rate of 10 °C min^{-1} with temperature ranged from 30 to600 °C under a nitrogen flow of 50 cm^3 min^{-1}. Empty cup was taken as a reference. The derivative of TGA (DTG) was obtained by differentials of TGA values and calculated using a central finite difference method as follows (Rhim et al., 2013):

$$\mathrm{DTG} = \frac{W_{t+\Delta t} - W_{t-\Delta t}}{2\Delta t}$$

where $W_{t+\Delta t} - W_{t-\Delta t}$ is the residual weight of sample at time $t + \Delta t$ and $t - \Delta t$, respectively, and Δt is the time interval for reading residual sample weight (Rhim, 2013). The maximum decomposition temperature (T_{max}) of films was calculated from DTG curve and the char content and the weight loss (%) was measured by TGA curve (Reddy & Rhim, 2014).

2.4.9. Antimicrobial activity

The antibacterial activities of neat agar and agar/CuNPs BNC films were examined as their inhibitory effects against the growth of Gram-positive bacteria, *L. monocytogenes* and Gram-negative bacteria, *E. coli*. Both the bacteria were supplied by the Korean culture collection center, Seoul, Korea. All the strains were aseptically inoculated in the TSB and BHI broth and subsequently incubated at 37 °C for 16 h. Inoculum of 100 μL was aseptically transferred to 50 mL TSB and BHI broth containing film samples (5 × 5 cm) and incubated at 37 °C for 12–16 h under mild shaking. The inhibitory effect was estimated periodically by measuring turbidity of the cultured medium at 600 nm using a spectrophotometer. Broth without film was taken as positive control and broths with respective films (without inoculum) was taken as negative control and used as blank for respective film samples. Antimicrobial tests were performed in triplicate with individually prepared films.

2.5. Statistical analysis

Statistical analysis was done by one-way analysis of variance (ANOVA), and the significance of each mean value was determined ($p < 0.05$) with the Duncan's multiple range tests using the SPSS software (SPSS Inc., Chicago, IL, USA).

3. Results and discussion

3.1. Optical properties and surface structure analysis

The optical properties of the synthesized CuNPs, neat agar film and agar/CuNPs BNC films were determined by measuring the absorption in range of 200–700 nm and transmittance at 280 and 660 nm. Fig. 1a and b shows the UV–visible absorption spectra of CuNPs, neat agar, and agar/CuNPs BNC films. The control agar film did not show any absorption peak in the scanned range of wavelength. The absorption spectra of CuA^{NaOH}, CuC^{NaOH}, and CuS^{NaOH} nanoparticles showed surface plasmonic resonance peaks at 290 and 360 nm, however, in the respective agar/CuNPs BNC films the peaks at 290 nm shifted to 270 nm, while the peaks at 360 nm were remained in the same position. The absorption spectra of CuA^{AA}, CuC^{AA}, and CuS^{AA} nanoparticles showed peaks at 250–270 nm, whereas, in the respective CuNPs/agar BNC films the absorption peaks were broader and shifted to 240 nm. Sutradhar et al. (2014) reported the absorption peaks of CuO nanoparticles at 271 and 269 nm synthesized by tea and coffee extract, respectively.

The protection of foodstuffs from the light, especially from UV radiation is one of the major functions required for food packaging films. The percent transmittance values of neat agar and agar/CuNPs BNC films are presented in Table 1. At a lower wavelength (280 nm) the control agar film showed the higher transmittance value (55.9 ± 0.7%), however, the UV light transmittance values decreased substantially after incorporation of CuNPs into the agar

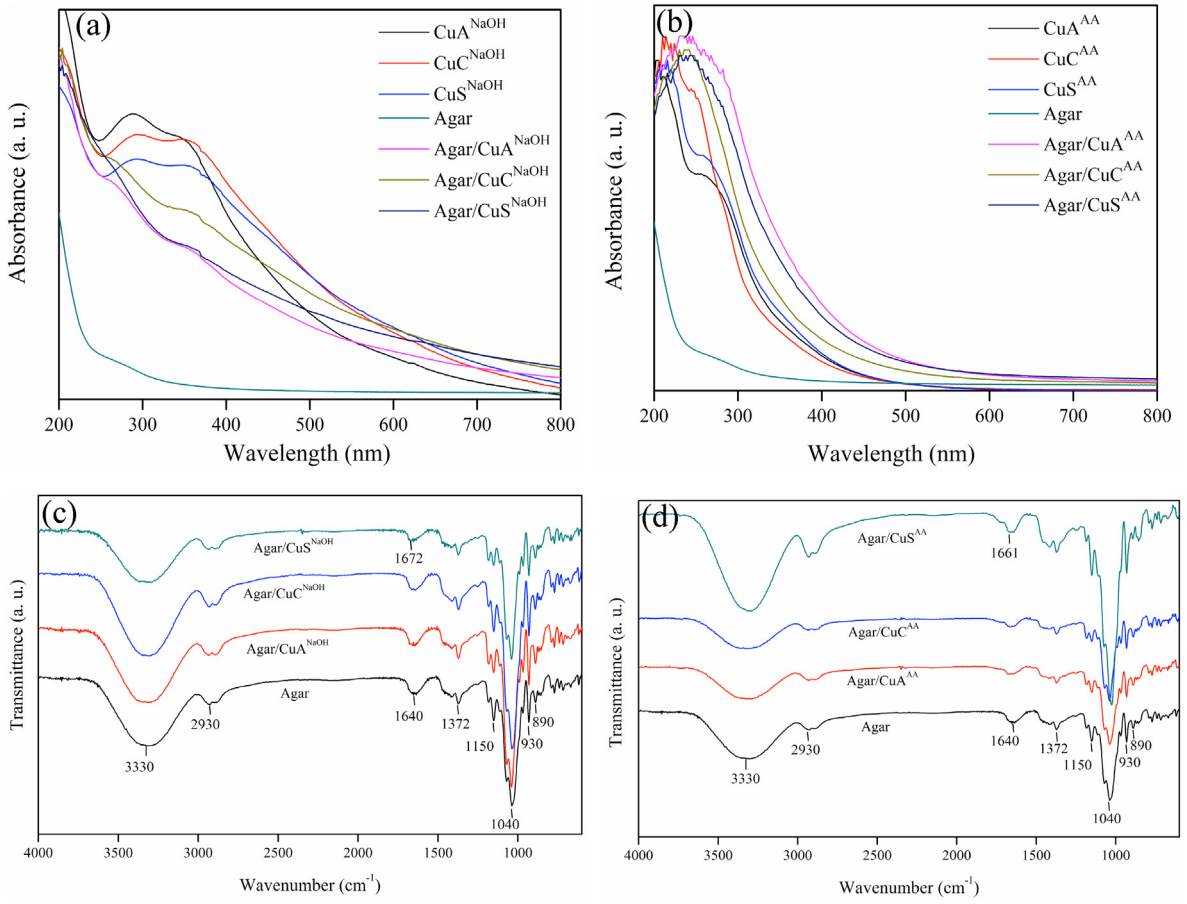

Fig. 1. UV–visible spectra of CuNPs, neat agar and agar/CuNPs BNC films (a and b). FTIR spectra of neat agar and agar/CuNPs BNC films (c and d).

Table 1
Color and percent transmittance of agar and agar/CuNPs composite films.

Film	L	a	b	ΔE	$T_{280\ nm}$ (%)	$T_{660\ nm}$ (%)
Agar	92.71 ± 0.31^{g}	-0.51 ± 0.01^{b}	4.90 ± 0.07^{a}	2.73 ± 0.26^{a}	55.9 ± 0.7^{f}	89.0 ± 0.3^{f}
Agar/CuA^{NaOH}	48.17 ± 1.30^{c}	8.16 ± 0.34^{e}	19.88 ± 0.33^{c}	50.15 ± 1.15^{e}	2.0 ± 0.3^{d}	50.7 ± 0.8^{c}
Agar/CuC^{NaOH}	41.28 ± 1.21^{a}	9.50 ± 0.30^{f}	16.71 ± 0.35^{b}	55.93 ± 1.12^{f}	1.5 ± 0.2^{c}	38.1 ± 1.4^{a}
Agar/CuS^{NaOH}	45.42 ± 1.45^{b}	7.84 ± 0.13^{e}	17.13 ± 0.32^{b}	51.51 ± 0.95^{e}	2.8 ± 0.2^{e}	45.5 ± 1.0^{b}
Agar/CuA^{AA}	71.27 ± 2.33^{d}	2.78 ± 0.99^{d}	30.38 ± 0.69^{f}	36.18 ± 2.12^{d}	0.1 ± 0.0^{a}	74.9 ± 1.5^{d}
Agar/CuC^{AA}	80.32 ± 0.66^{f}	-1.19 ± 0.15^{a}	24.66 ± 0.69^{d}	26.02 ± 0.92^{b}	0.5 ± 0.1^{b}	81.1 ± 0.5^{e}
Agar/CuS^{AA}	73.80 ± 0.61^{e}	1.66 ± 0.27^{c}	29.35 ± 0.38^{e}	33.68 ± 0.68^{c}	0.1 ± 0.0^{a}	74.7 ± 1.8^{d}

Values with the same superscript letter in the same column indicate that they are not statistically different ($p < 0.05$).

films. Agar/CuA^{AA}, agar/CuC^{AA}, and agar/CuS^{AA} BNC films transmitted less UV light (0.5–1.0%) compared to that of agar/CuA^{NaOH}, agar/CuC^{NaOH}, and agar/CuS^{NaOH} BNC films (1.5–2.8%). These results indicate that the CuNPs incorporated into agar have strong UV light screening function. The percent light transmittance of control agar film at visible region (660 nm) was 89.0 ± 0.3 (Table 1), which indicates that the control agar film is very clear and transparent. The light transmittance at 660 nm decreased after incorporation of CuNPs. The light transmittance was observed less in agar/CuA^{NaOH}, agar/CuC^{NaOH}, and agar/CuS^{NaOH} BNC films (38.1–50.7%) as compared to agar/CuA^{AA}, agar/CuC^{AA}, and agar/CuS^{AA} BNC films (74.7–81.1%). Among all agar/CuNPs BNC films, agar/CuC^{AA} showed the highest light transmittance (81.1 ± 0.5%) at 660 nm which suggests that the transparency of agar/CuC^{AA} film has not been sacrificed significantly even though UV screening increased profoundly ($T_{280} = -0.1 \pm 0.5$%).

FE-SEM micrographs showed the surface morphology of neat agar and agar/CuNPs BNC films (Fig. 2). The micrographs of corresponding CuNPs are presented as figure insert. Smooth and compact surface morphology was observed in the neat agar film, while agar/CuNPs BNC films showed rough surface structures with evenly distributed CuNPs. The results showed that the CuNPs were homogeneously distributed on the surface as well as embedded in the agar matrix through the whole film. They also exhibited the presence of CuNPs with different shapes depends on the type of nanoparticles used. Some aggregations of CuNPs were also observed on the film surfaces. Kanmani and Rhim (2014b) observed a similar pattern of surface when ZnO nanoparticles were incorporated into the agar.

3.2. FT-IR and XRD analysis

The FT-IR spectra of neat agar and agar/CuNPs BNC films displayed characteristic peaks in the range of 3500–650 cm^{-1} (Fig. 1c and d). In agar film, the characteristic broad absorption band at about 3330 cm^{-1} was attributed to the stretching of hydroxyl (O–H)

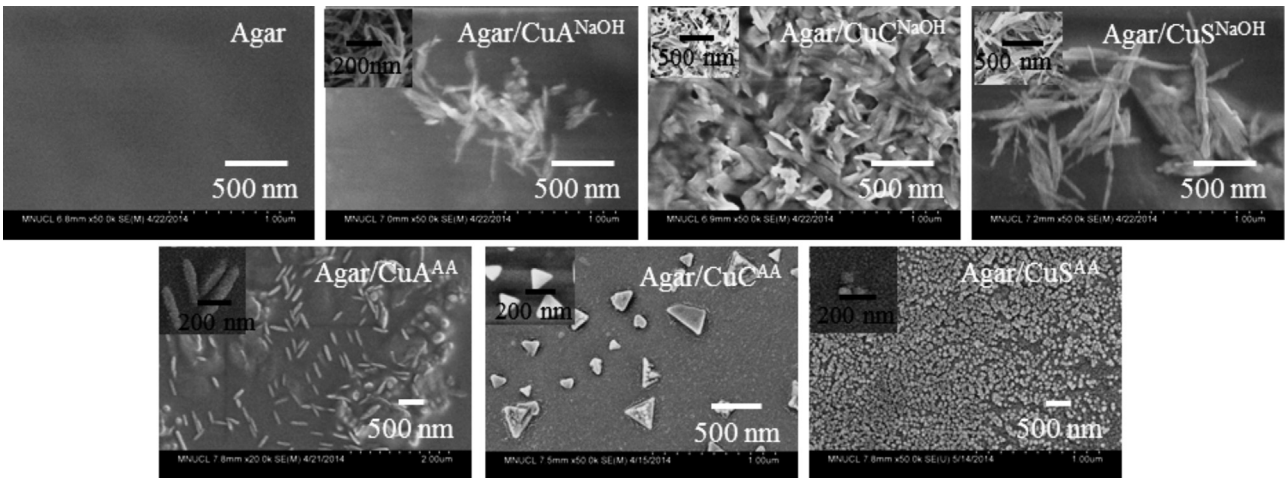

Fig. 2. FE-SEM micrographs of neat agar and agar/CuNPs BNC films. Inserts show the FE-SEM micrographs of corresponding CuNPs used for reinforcement in agar matrix.

groups (Wu, Geng, Chang, Yu, & Ma, 2009). The peak around 2930 was observed due to C–H stretching of methane. The peak at 1640 cm^{-1} was attributed to the stretching vibration of the conjugated peptide bond formation by amine (NH) and acetone groups in agar (Kanmani & Rhim, 2014a). The peak at 1372 cm^{-1} was attributed to an ester sulfate group (Volery, Besson, & Schaffer-lequart, 2004). The characteristic peaks at 1040 and 930 cm^{-1} indicated C–O stretching group of 3,6-anhydrogalactose. Similar peaks with high or low intensities compared to neat agar film were observed in agar/CuNPs BNC films, which suggest that there were no chemical interactions between agar and CuNPs. The FR-IR results suggest that CuNPs has a good compatibility with agar.

The X-ray diffraction (XRD) pattern of neat agar and agar/CuNPs BNC films are presented in Fig. 3. The neat agar film did not show any diffraction peak in the scanned range of $2\theta = 30–80^{\circ}$. However, agar/CuNPs BNC films exhibited characteristic peaks at 2θ values depended on the types of CuNPs used for reinforcement. The presence of these peaks confirmed the crystalinity of CuNPs used in the present study (Ahmed, Alhadlaq, Khan, Karuppiah, & Al-Dhabi, 2014; Das, Kalita, Gogoi, Buragohain, & Karak, 2014).

3.3. Thermal analysis

Thermal stability of neat agar and agar/CuNPs BNC films was tested using TGA analysis and the results are presented in Fig. 4. TGA curves show the weight loss pattern on thermal decomposition of the films (Fig. 4a and b). DTG curves clearly show the maximum decomposition temperature at each step of thermal decomposition (Fig. 4c and d). All the films exhibited multiple steps of thermal degradation. The initial weight loss for all films was observed around 90 °C, which was due to the removal of moisture from the films, which accounted for about 5–10% of weight loss (Rhim, 2013). The subsequent steps of degradation were varied depending on the film types. The second decomposition begins at around 200 °C and reached a maximum around 250 °C ascribed to the volatilization of glycerol added as a plasticizer (Martucci & Ruseckaite, 2010). The third steps of major thermal decomposition were observed around 300 °C and can be attributed to the thermal decomposition of agar used as polymer (El-Hefian, Nasef, & Yahaya, 2012). After the final thermal decomposition, the residual percentages at around 600 °C of the neat agar, agar/CuA^{NaOH}, agar/CuC^{NaOH}, agar/CuS^{NaOH}, agar/CuA^{AA}, agar/CuC^{AA}, and agar/CuS^{AA} BNC films were 24.96, 25.39, 25.50, 24.72, 23.83, 24.87, and 26.87%, respectively. The pattern of degradation was similar for agar and agar/CuA^{NaOH}, agar/CuC^{NaOH}, and agar/CuS^{NaOH} BNC films, however, variations were observed in agar/CuA^{AA}, agar/CuC^{AA}, and agar/CuS^{AA} BNC films. The results show that agar/CuA^{AA}, agar/CuC^{AA}, and agar/CuS^{AA} BNC films were more thermostable as compared to neat agar film. Similar results were obtained when ZnO nanoparticles were incorporated in agar bio-nanocomposite films (Kanmani & Rhim, 2014b).

3.4. Antimicrobial activity

Antimicrobial activity of neat agar and agar/CuNPs BNC films was tested against Gram-positive and Gram-negative food-borne pathogenic bacteria using increase in turbidity (OD_{600nm}) method and the results are presented in Fig. 5. All the BNC films incorporated with CuNPs exhibited strong antimicrobial activity against both, Gram-positive and Gram-negative bacteria, however, as expected, the neat agar film did not show any antimicrobial activity. The turbidity (OD_{600nm}) was increased in the control (inoculum without any film) and neat agar film and log phase reached at 4 and 8 h in Gram-negative and Gram-positive bacteria, respectively, however, stationary phase was reached after 8 and 16 h, respectively. The optical density did not increase in any sample containing agar/CuNPs BNC films. It was expected that the nano size of the CuNPs, relatively high surface area and high dispersion of CuNPs in agar matrices interact closely with the bacterial cells leading to inhibition of bacteria. The inhibition of bacterial growth by CuNPs could be due to inhibition of DNA replication (Feng et al., 2000) and destruction of the cell wall of bacteria (Singh, Singh, Prasad, & Gambhir, 2008).

3.5. Moisture content, water vapor permeability, and water contact angle

Table 2 shows the MC, WVP, and WCA of the neat agar and agar/CuNPs BNC films. The neat agar and CuC^{AA} agar film showed lower MC compared to other agar/CuNPs BNC films. This is probably due to the addition of nanoparticles reduces the interaction between polymer chains, thereby making more availability of free hydroxyl groups to absorb water. The WVP of agar film was 1.14×10^{-9} g m m^{-2} Pa^{-1} s^{-1}, which were lower than the previously reported values (Rhim, 2012). This lower in WVP might be due to the use of an amount of glycerol as plasticizer. The higher the concentration of glycerol, the higher will be the value of WVP. In the present study, 30 wt% glycerol was used as compared to 50 wt% used in the previous study (Rhim, 2012). In general, addition of plasticizers increase gas, water vapor and solute permeability of the film

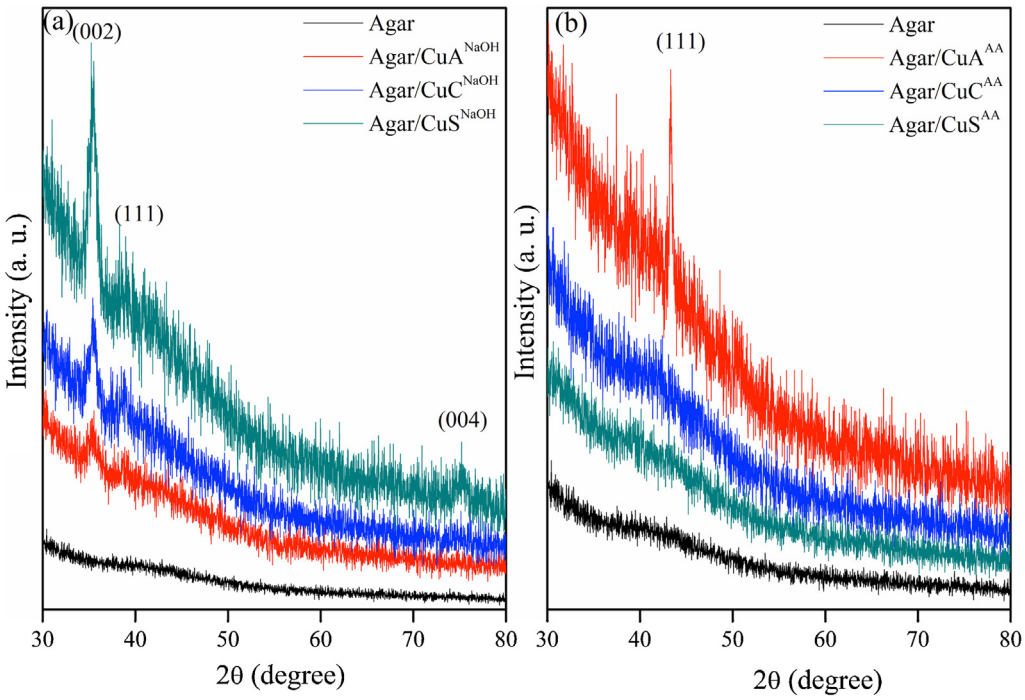

Fig. 3. X-ray diffraction (XRD) patterns of the neat agar and agar/CuNPs BNC films.

(Gontard, Guilbert, & Cuq, 1993). There was no significant ($p > 0.05$) difference observed in WVP of the neat agar and agar/CuNPs BNP films. However, WCA of all agar/CuNPs BNC films was increased significantly compared with the neat agar film except agar/CuA^{AA}, where, WCA values decreased as compared to the neat agar film. WCA is one of the basic wetting properties of packaging materials, which is usually used as an indicator for hydrophilic/hydrophobic properties of the film surface. The WCA of the control agar film was

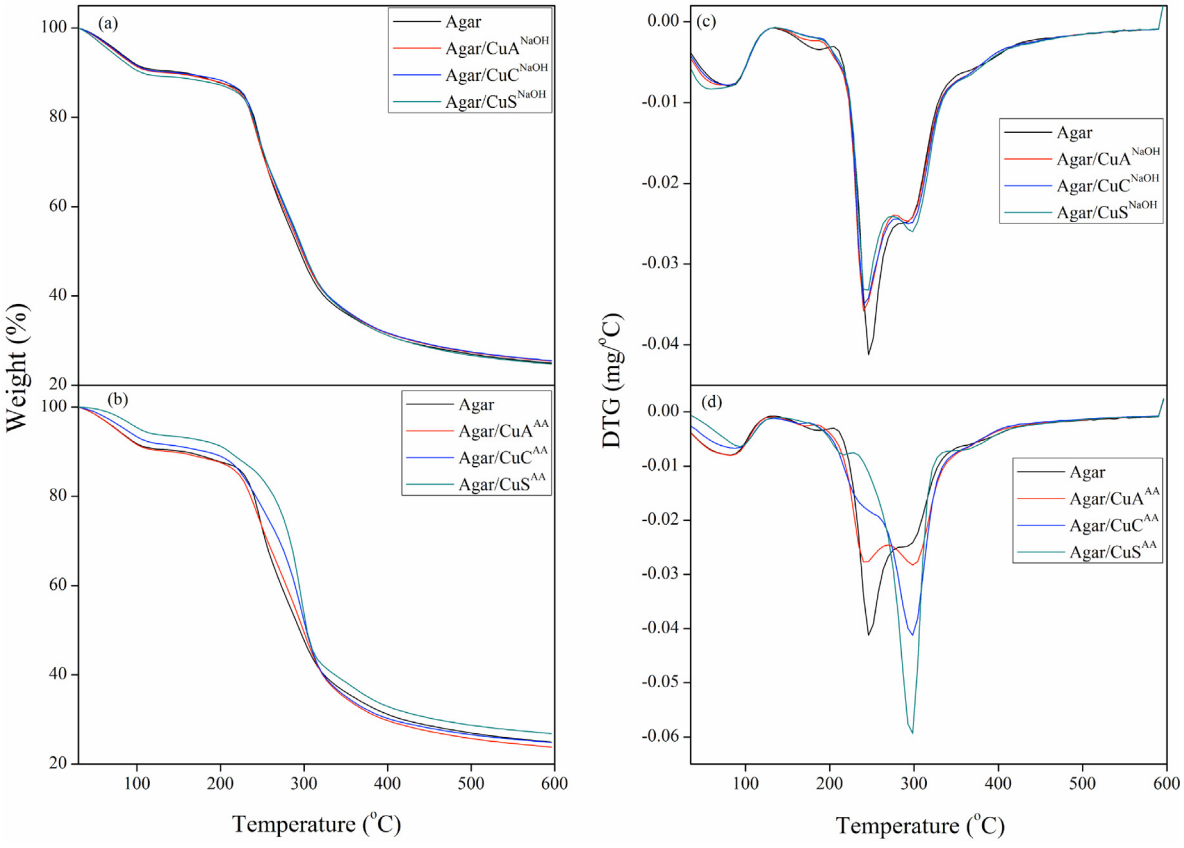

Fig. 4. TGA thermograms and DTG curves of neat agar and agar/CuNPs BNC films.

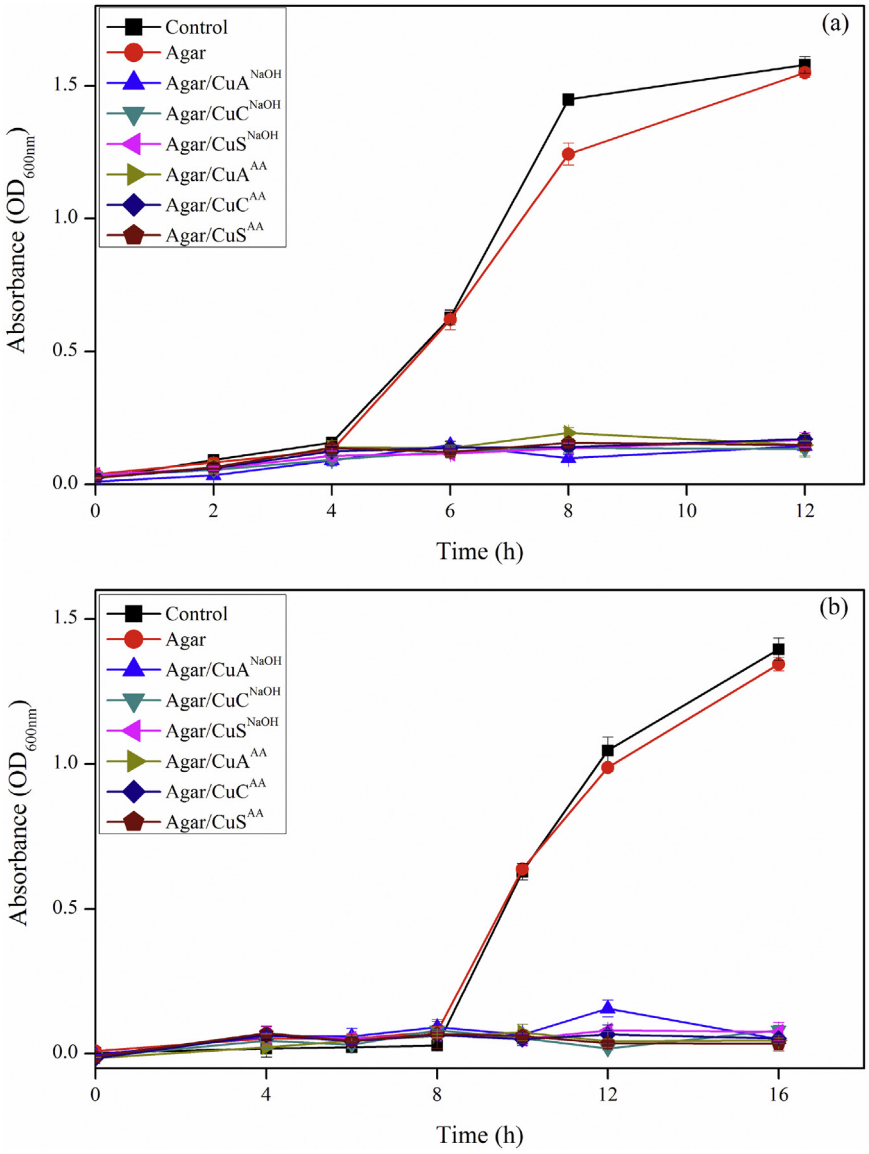

Fig. 5. Antimicrobial activity of neat agar and agar/CuNPs BNC films against (a) *E. coli* and (b) *L. monocytogenes*.

Table 2
Moisture content, water vapor permeability, and water contact angle of agar and agar/CuNPs composite films.

Film	MC (%)	WVP ($\times 10^{-9}$ g m m^{-2} Pa^{-1} s^{-1})	WCA (°)
Agar	12.2 ± 0.7^{ab}	1.14 ± 0.07^{abc}	45.3 ± 2.3^{b}
Agar/CuA^{NaOH}	12.9 ± 0.4^{cd}	0.96 ± 0.08^{a}	60.3 ± 1.5^{e}
Agar/CuC^{NaOH}	12.4 ± 0.4^{abc}	1.10 ± 0.03^{ab}	53.4 ± 2.4^{d}
Agar/CuS^{NaOH}	13.6 ± 0.2^{d}	1.09 ± 0.02^{ab}	59.8 ± 0.6^{e}
Agar/CuA^{AA}	12.6 ± 0.3^{bc}	1.36 ± 0.18^{c}	39.9 ± 0.6^{a}
Agar/CuC^{AA}	11.8 ± 0.3^{a}	1.13 ± 0.13^{ab}	49.4 ± 0.7^{c}
Agar/CuS^{AA}	12.8 ± 0.0^{bc}	1.30 ± 0.21^{bc}	49.8 ± 1.5^{c}

Values with the same superscript letter in the same column indicate that they are not statistically different ($p < 0.05$).

$45.3 \pm 2.33°$, which is consistent with previously reported value of $46.9 \pm 3.40°$ for an agar film (Rhim et al., 2013). The increase in WCA values of agar/CuNPs BNC films indicates that the surface hydrophobicity of CuNPs blended agar films increased. The increase in the WCA of the agar/CuNPs BNC films was attributed to the inclusion of hydrophobic metallic CuNPs in the polymer matrix resulting in the increased surface hydrophobicity of the agar/CuNPs BNC films. Similar results for WCA were obtained when silver nanoparticles were blended in agar film (Rhim et al., 2013).

3.6. Thickness and mechanical properties

The mechanical properties of neat agar and agar/CuNPs BNC films are shown in Table 3. The film thickness was not affected significantly ($p > 0.05$) upon addition of CuNPs. Similar results were obtained when silver nanoparticles were blended in agar film (Rhim et al., 2013). TS of the neat agar film was 45.8 ± 2.9 MPa, which was much higher than the previously reported value (Rhim, 2012). This difference is mainly attributed to the amount of glycerol used as a plasticizer. No significant change in TS was observed in agar/CuNPs BNC films. The lowest value of TS was obtained in agar/CuA^{AA} film (38.8 ± 2.7 MPa), which is around 15% lower than the value obtained in neat agar film. The stiffness and flexibility of the films were determined by the Young's modulus (EM, GPa) and elongation at break (E, %), respectively. There was no significant decrease in stiffness and flexibility observed in BNC films after incorporation of different shapes and sizes of CuNPs.

Table 3
Thickness and tensile properties of agar and agar/CuNPs composite films.

Film	Thickness (μm)	TS (MPa)	*E* (%)	EM (GPa)
Agar	45.9 ± 1.7^{cd}	45.8 ± 2.9^{b}	13.9 ± 3.4^{ab}	1.63 ± 0.11^{e}
Agar/CuA^{NaOH}	44.4 ± 2.1^{abc}	49.2 ± 3.7^{c}	13.8 ± 3.1^{ab}	1.82 ± 0.11^{f}
Agar/CuC^{NaOH}	44.1 ± 2.1^{ab}	44.9 ± 3.6^{b}	16.3 ± 3.3^{b}	1.61 ± 0.13^{de}
Agar/CuS^{NaOH}	45.8 ± 2.1^{bcd}	39.0 ± 3.6^{a}	16.4 ± 4.5^{b}	1.34 ± 0.17^{a}
Agar/CuA^{AA}	46.6 ± 2.9^{d}	38.8 ± 2.7^{a}	13.7 ± 3.2^{a}	1.44 ± 0.05^{b}
Agar/CuC^{AA}	44.9 ± 2.9^{abcd}	39.4 ± 2.8^{a}	12.9 ± 2.9^{a}	1.53 ± 0.10^{cd}
Agar/CuS^{AA}	43.5 ± 1.4^{a}	39.5 ± 1.9^{a}	13.9 ± 2.5^{ab}	1.51 ± 0.10^{bc}

Values with the same superscript letter in the same column indicate that they are not statistically different ($p < 0.05$).

4. Conclusion

Six different types of CuNPs were prepared by reducing three different copper salts using two reducing agents and they were used as reinforcing materials for the synthesis of agar/CuNPs BNC films. The CuNPs/agar BNC films exhibited profound UV light absorbing and antimicrobial activity without sacrificing the transparency and mechanical properties of the films. All the agar/CuNPs BNC films exhibited strong antimicrobial activity against both Gram-positive and Gram-negative food-borne pathogens. To the best of our knowledge, the present work is the first research work performed in the preparation of biopolymer-based antimicrobial BNC film using CuNPs. The agar/CuNPs BNC films with UV barrier and antimicrobial functions have a high potential as environmentally friendly food packaging films, especially, in the application for the UV screening packaging and antimicrobial food packaging systems. The antimicrobial packaging systems are highly useful to minimize the growth of post-processing contamination, extending food shelf-life and improving food safety. The profound UV barrier property of the CuNPs included films have a high potential for the application as UV protective packaging films for UV-sensitive foods such as potato. In addition, the high thermal stability of the metal oxide nanoparticles can be explored for the industrial extrusion processing of composite with CuNPs. Nevertheless, further research works are needed for the industrial production of CuNPs included nanocomposite materials.

Acknowledgement

This research was supported by the Agriculture Research Center (ARC 710003) program of the Ministry for Agriculture, Food and Rural Affairs, Korea.

References

Ahamed, M., Alhadlaq, H. A., Khan, M. A. M., Karuppiah, P., & Al-Dhabi, N. A. (2014). Synthesis, characterization, and antimicrobial activity of copper oxide nanoparticles. *Journal of Nanomaterials*, http://dx.doi.org/10.1155/2014/637858

Borkow, G., & Gabbay, J. (2009). Copper, an ancient remedy returning to fight microbial, fungal and viral infections. *Current Chemical Biology*, *3*, 272–278.

Cárdenas, G., Díaz, J. V., Meléndrez, M. F., Cruzat, C. C., & García, A. C. (2009). Colloidal Cu nanoparticles/chitosan composite film obtained by microwave heating for food package applications. *Polymer Bulletin*, *62*, 511–524.

Dang, T. M. D., Le, T. T. T., Fribourg-Blanc, E., & Dang, M. C. (2011). Synthesis and optical properties of copper nanoparticles prepared by a chemical reduction method. *Advances in Natural Sciences: Nanoscience and Nanotechnology*, *2*, 15009–15014.

Das, G., Kalita, R. D., Gogoi, P., Buragohain, A. K., & Karak, N. (2014). Antibacterial activities of copper nanoparticle-decorated organically modified montmorillonite/epoxy nanocomposites. *Applied Clay Science*, *90*, 18–26.

Drelich, J., Li, B., Bowen, P., Hwang, J. Y., Mills, O., & Hoffman, D. (2011). Vermiculite decorated with copper nanoparticles: novel antibacterial hybrid material. *Applied Surface Science*, *257*, 9435–9443.

Duncan, T. V. (2011). Application of nanotechnology in food packaging and food safety: barrier materials, antimicrobials and sensors. *Journal of Colloid and Interface Science*, *363*, 1–24.

El-Hefian, E. A., Nasef, M. M., & Yahaya, A. H. (2012). Preparation and characterization of chitosan/agar blended films: Part 2. Thermal, mechanical, and surface properties. *E-Journal of Chemistry*, *9*, 510–516.

Feng, Q. L., Wu, J., Chen, G. Q., Cui, F. Z., Kim, T. N., & Kim, J. O. (2000). A mechanistic study of the antibacterial effect of silver ions on *Escherichia coli* and *Staphylococcus aureus*. *Journal of Biomedical Materials Research*, *52*, 662–668.

Gennadios, A., Weller, C. L., & Gooding, C. H. (1994). Measurement errors in water vapor permeability of highly permeable, hydrophilic edible films. *Journal of Food Engineering*, *21*, 395–409.

Gong, P., Li, H., He, X., Wang, K., Hu, J., Tan, W., Zhang, S., & Yang, X. (2007). Preparation and antibacterial activity of Fe_3O_4@Ag nanoparticles. *Nanotechnology*, *18*, 604–611.

Gontard, N., Guilbert, S., & Cuq, J. L. (1993). Water and glycerol as plasticizers affect mechanical and water vapor barrier properties of an edible wheat gluten film. *Journal of Food Science*, *58*, 206–211.

Hostynek, J. J., & Maibach, H. I. (2004). Copper hypersensitive: Dermatologic aspects. *Dermatology and Therapy*, *17*, 328–333.

Huang, H. H., Yan, F. Q., Kek, Y. M., Chew, C. H., Xu, G. Q., Ji, W., Oh, P. S., & Tang, S. H. (1997). Synthesis, characterization, and nonlinear optical properties of copper nanoparticles. *Langmuir*, *13*, 172–175.

Kanmani, P., & Rhim, J. W. (2014a). Antimicrobial and physical-mechanical properties of agar-based films incorporated with grapefruit seed extract. *Carbohydrate Polymers*, *102*, 708–716.

Kanmani, P., & Rhim, J. W. (2014b). Properties and characterization of bionanocomposite films prepared with various biopolymers and ZnO nanoparticles. *Carbohydrate Polymers*, *106*, 190–199.

Kyriacou, S. V., Brownlow, W. J., & Xu, X. H. (2004). Using nanoparticle optics assay for direct observation of the function of antimicrobial agents in single live bacterial cells. *Biochemistry*, *43*, 140–147.

Liu, Z., & Bando, Y. (2003). A novel method for preparing copper nanorods and nanowires. *Advanced Materials*, *15*, 303–305.

Magdassi, S., Grouchko, M., & Kamyshny, A. (2010). Copper nanoparticles for printed electronics: Routes towards achieving oxidation stability. *Materials*, *3*, 4626–4638.

Martucci, J. F., & Ruseckaite, R. A. (2010). Three-layer sheets based on gelatin and poly(lactic acid), Part 1: Preparation and properties. *Journal of Applied Polymer Science*, *118*, 3102–3110.

Mary, G., Bajpai, S. K., & Chand, N. (2009). Copper (II) ions and copper nanoparticles-loaded chemically modified cotton cellulose fibers with fair antibacterial properties. *Journal of Applied Polymer Science*, *113*, 757–766.

Reddy, J. P., & Rhim, J. W. (2014). Characterization of bionanocomposite films prepared with agar and paper-mulberry pulp nanocellulose. *Carbohydrate Polymers*, *110*, 480–488.

Rhim, J. W. (2012). Water vapor adsorption isotherms of agar-based nanocomposite films. *Journal of Food Science*, *77*, N68–N72.

Rhim, J. W. (2013). Effect of PLA lamination on performance characteristics of agar/κ-carrageenan/clay bio-nanocomposite film. *Food Research International*, *51*, 714–722.

Rhim, J. W., Hong, S. I., Park, H. M., & Ng, P. K. W. (2006). Preparation and characterization of chitosan-based nanocomposite films with antimicrobial activity. *Journal of Agricultural and Food Chemistry*, *54*, 5814–5822.

Rhim, J. W., & Wang, L. F. (2013). Mechanical and water barrier properties of agar/κ-carrageenan/konjac glucomannan ternary blend biohydrogel films. *Carbohydrate Polymers*, *96*, 71–81.

Rhim, J. W., Wang, L. F., & Hong, S. I. (2013). Preparation and characterization of agar/silver nanoparticles composite films with antimicrobial activity. *Food Hydrocolloids*, *33*, 327–335.

Shankar, S., & Rhim, J. W. (2014). Effect of copper salts and reducing agents on characteristics and antimicrobial activity of copper nanoparticles. *Materials Letters*, http://dx.doi.org/10.1016/j.matlet.2014.06.014

Singh, M., Singh, S., Prasad, S., & Gambhir, I. S. (2008). Nanotechnology in medicine and antibacterial effect of silver nanoparticles. *Digest Journal of Nanomaterials and Biostructures*, *3*, 115–122.

Sutradhar, P., Saha, M., & Maiti, D. (2014). Microwave synthesis of copper oxide nanoparticles using tea leaf and coffee powder extracts and its antibacterial activity. *Journal of Nanostructure in Chemistry*, *4*, 86–91.

Tilaki, R. M., Iraji zad, A., & Mahdavi, S. M. (2007). Size, composition and optical properties of copper nanoparticles prepared by laser ablation in liquids. *Applied Physics A*, *88*, 415–419.

Tunc, S., & Duman, O. (2011). Preparation of active antimicrobial methyl cellulose/carvacrol/montmorillonite nanocomposite films and investigation of carvacrol release. *LWT - Food Science and Technology*, *44*, 465–472.

Vellora, V., Padil, T., & Černík, M. (2013). Green synthesis of copper oxide nanoparticles using gum karaya as a biotemplate and their antibacterial application. *International Journal of Nanomedicine*, *8*, 889–898.

Volery, P., Besson, R., & Schaffer-lequart, C. (2004). Characterization of commercial carrageenans by Fourier transform infrared spectroscopy using single-reflection attenuated total reflection. *Journal of Agricultural and Food Chemistry*, *52*, 7457–7463.

Wu, Y., Geng, F., Chang, P. R., Yu, J., & Ma, X. (2009). Effect of agar on the microstructure and performance of potato starch film. *Carbohydrate Polymers*, *76*, 299–304.